Manuscript submitted to
AIMS' Journals
Volume **X**, Number **0X**, XX **200X**

Website: http://AIMsciences.org

pp. **X–XX**

AN ENTROPY BASED THEORY OF THE GRAIN BOUNDARY CHARACTER DISTRIBUTION

K. Barmak

Department of Materials Science and Engineering, Carnegie Mellon University, Pittsburgh, PA 15213

E. Eggeling

Fraunhofer Institut Computer Graphics Research IGD, Project Group Graz, A-8010 Austria

M. Emelianenko

Department of Mathematical Sciences, George Mason University, Fairfax, VA 22030

Y. Epshteyn

Department of Mathematics, The University of Utah, Salt Lake City, UT, 84112

D. Kinderlehrer

Department of Mathematical Sciences, Carnegie Mellon University, Pittsburgh, PA 15213

R. Sharp

Department of Mathematical Sciences, Carnegie Mellon University, Pittsburgh, PA 15213

S. Ta'asan

Department of Mathematical Sciences, Carnegie Mellon University, Pittsburgh, PA 15213

(Communicated by the associate editor name)

Abstract. Cellular networks are ubiquitous in nature. They exhibit behavior on many different length and time scales and are generally metastable. Most technologically useful materials are polycrystalline microstructures composed of a myriad of small monocrystalline grains separated by grain boundaries. The energetics and connectivity of the grain boundary network plays a crucial role in determining the properties of a material across a wide range of scales. A central problem in materials science is to develop technologies capable of producing an arrangement of grains—a texture—appropriate for a desired set of material properties. Here we discuss the role of energy in texture development, measured by a character distribution. We derive an entropy based theory based on a mass transport and a Kantorovich-Rubinstein-Wasserstein metric to suggest that, to first approximation, this distribution behaves like the solution to a Fokker-Planck Equation.

2000 *Mathematics Subject Classification.* Primary: 37M05, 35Q80, 93E03, 60J60, 35K15, 35A15.

Key words and phrases. Coarsening, Texture Development, Large Metastable Networks, Critical Event Model, Entropy Based Theory, Free Energy, Fokker-Planck Equation, Kantorovich-Rubinstein-Wasserstein Metric .

Research supported by NSF DMR0520425, DMS 0405343, DMS 0305794, DMS 0806703, DMS 0635983, DMS 0915013.

Contents

1. Introduction 2
2. Mesoscale theory 4
3. Discussion of the Simulation 6
4. Simplified coarsening model 8
4.1. Formulation 9
4.2. Mass transport paradigm 12
5. Validation of the scheme 15
6. The entropy method for the GBCD 17
7. Discussion/conclusions 21
8. Appendix: The Kantorovich-Rubinstein-Wasserstein (KRW) implicit scheme for Fokker-Planck Equation and the asymptotic behavior 22
8.1. The KRW implicit scheme for the Fokker-Planck Equation 22
8.2. Asymptotic behavior 22
Acknowledgements 25
REFERENCES 25

1. **Introduction.** Cellular networks are ubiquitous in nature. They exhibit behavior on many different length and time scales and are generally metastable. Most technologically useful materials are polycrystalline microstructures composed of a myriad of small monocrystalline grains separated by grain boundaries, and thus comprise cellular networks. The energetics and connectivity of the grain boundary network plays a crucial role in determining the properties of a material across a wide range of scales. A central problem in materials is to develop technologies capable of producing an arrangement of grains that provides for a desired set of material properties. Traditionally the focus has been on the geometric feature of size and the preferred distribution of grain orientations, termed texture. More recent mesoscale experiment and simulation permit harvesting large amounts of information about both geometric features and crystallography of the boundary network in material microstructures, [2],[1],[40],[53],[54]

The grain boundary character distribution (GBCD) is an empirical distribution of the relative length (in 2D) or area (in 3D) of interface with a given lattice misorientation and grain boundary normal. It is a leading candidate to characterize texture of the boundary network [40]. During the growth process, an initially random grain boundary texture reaches a steady state that is strongly correlated to the interfacial energy density. In simulation, a GBCD is always found.

In the special situation where the given energy depends only on lattice misorientation, the steady state GBCD and the interfacial energy density are related by a Boltzmann distribution. This is among the simplest non-random distributions, corresponding to independent trials with respect to the density. It offers compelling evidence that the GBCD is a material property. Thus experimental measures of the GBCD, rather than being anecdotal, are trials for the ideal distribution. Why does such a simple distribution arise from such a complex system?

We outline a new entropy based theory which suggests that the evolving GBCD satisfies a Fokker-Planck Equation. Coarsening in polycrystalline systems is a complicated process involving details of material structure, chemistry, arrangement of grains in the configuration, and environment. In this context, we consider just two

competing global features, as articulated by C. S. Smith [56]: cell growth according to a local evolution law and space filling constraints. We shall impose curvature driven growth for the local evolution law, cf. Mullins [50]. Space filling requirements are managed by critical events, rearrangements of the network involving deletion of small contracting cells and facets. The interaction between the evolution law and the constraints is, we shall discover, governed primarily by the balance of forces at triple junctions. This balance of forces, often referred to as the Herring Condition [32], is the natural boundary condition associated with the equations of curvature driven growth. It determines a dissipation relation for the network as a whole.

In our view this is a question in large scale computation and our theory will be derived with the simulation of coarsening in mind. Numerical simulations have been established as a major tool in the analysis of many physical systems for a long time, see for example [60],[44],[45],[26],[27],[21],[58],[57],[42],[52],[23],[46],[48]. However, the idea of large scale computation as the essential method for the modeling and comprehension of large complex systems is relatively new. Porous media and groundwater flow is an important case of this, see for example [31],[5],[4],[7],[6]. For coarsening of cellular systems, it is a natural approach as well. The laboratory is the venue to assess the validity of the local evolution law. Once this law is adopted, we appeal to simulation, since we cannot control all the other elements present in the experimental system, many of which are unknown. On the other hand, *in silico* we may exercise precise control of the variables appropriate to the evolution law and the constraint.

There are many large scale metastable material systems, for example, magnetic hysteresis, [16], and second phase coarsening, [47],[61]. In these, the theory is based on mesoscopic or macroscopic variables simply abstracting the role of the smaller scale elements of the system. There is no general 'multiscale' framework for upscaling from the local behavior of individual cells to behavior of the network when they interact and change their character. So we must attempt to tease the system level information from the many coupled elements of which it consists.

Our strategy is to introduce a simplified coarsening model that is driven by the boundary conditions that reflects the dissipation relation of the grain growth system. It resembles an ensemble of inertia-free spring-mass-dashpots. For this simpler network, we learn how entropic or diffusive behavior at the large scale emerges from a dissipation relation at the scale of local evolution. The cornerstone is our novel implementation of the iterative scheme for the Fokker-Planck Equation in terms of the system free energy and a Kantorovich-Rubinstein-Wasserstein metric [37], cf. also [36], which will be defined and explained later in the text. The network level nonequlibrium nature of the iterative scheme leaves free a temperature-like parameter. The entropy method is exploited to identify uniquely this parameter. To illustrate the idea, we include a simple application to the solution of the Fokker-Planck Equation itself.

We present evidence that the theory predicts the results of large scale 2D simulations [10]. Energy densities consisting of quadratic and quartic trigonometric polynomials are analyzed in detail. The discussion of the quartic based energy density places in relief the entropic nature of the GBCD. For consistency with experiment we refer to [40]. A companion paper emphasizing the materials aspects of this project is [9]. A theory for the evolution of geometric features of microstructure is discussed in [14, 22]. Some of the results of the present work were announced

in [8],[10]. Different treatments of texture development are given in [28],[29] and [34],[49].

2. **Mesoscale theory.** Our point of departure is the common denominator theory for the mesoscale description of microstructure. This is growth by curvature, the Mullins Equation (2.2) below, for the evolution of curves or arcs individually or in a network, which we employ for our local law of evolution. Boundary conditions must be imposed where the arcs meet. This condition is the Herring Condition, (2.3), which is the natural boundary condition at equilibrium for the Mullins Equation. Since their introduction by Mullins, [50], and Herring, [32], [33], a large and distinguished body of work has grown about these equations. Most relevant to here are [30], [20], [39], [51]. Let α denote the misorientation between two grains separated by an arc Γ, as noted in Figure 1, with normal $n = (\cos\theta, \sin\theta)$, tangent direction b and curvature κ. Let $\psi = \psi(\theta, \alpha)$ denote the energy density on Γ. So

$$\Gamma : x = \xi(s,t), \quad 0 \leqq s \leqq L, \ t > 0, \tag{2.1}$$

with

$$b = \frac{\partial \xi}{\partial s} \text{ (tangent) and } \ n = Rb \text{ (normal)}$$
$$v = \frac{\partial \xi}{\partial t} \text{ (velocity) and } v_n = v \cdot n \text{ (normal velocity)}$$

where R is a positive rotation of $\pi/2$. The Mullins Equation of evolution is

$$v_n = (\psi_{\theta\theta} + \psi)\kappa \text{ on } \Gamma. \tag{2.2}$$

We assume that only triple junctions are stable and that the Herring Condition

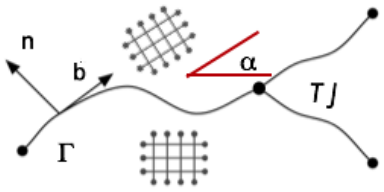

FIGURE 1. An arc Γ with normal n, tangent b, and lattice misorientation α, illustrating lattice elements.

holds at triple junctions. This means that whenever three curves $\{\Gamma^{(1)}, \Gamma^{(2)}, \Gamma^{(3)}\}$, meet at a point p the force balance, (2.3) below, holds:

$$\sum_{i=1,..,3} (\psi_\theta n^{(i)} + \psi b^{(i)}) = 0. \tag{2.3}$$

It is easy to check that the instantaneous rate of change of energy of Γ is

$$\frac{d}{dt}\int_\Gamma \psi|b|ds = -\int_\Gamma v_n^2 ds + v \cdot (\psi_\theta n + \psi b)|_{\partial\Gamma} \tag{2.4}$$

We turn now to a network of grains bounded by $\{\Gamma_i\}$ subject to some condition at the border of the region they occupy, like fixed end points or periodicity, cf. Figure 2. Our simulation is described in [41],[38]. The typical simulation consists in initializing a configuration of cells and their boundary arcs, usually by a modified

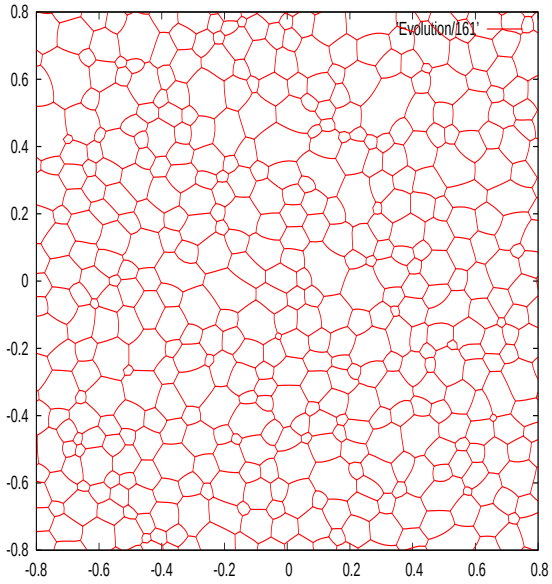

FIGURE 2. Example of an instant during the simulated evolution of a cellular network. This is from a small simulation with constant energy density and periodic conditions at the border of the configuration.

Voronoi tessellation, and then solving the system (2.2), (2.3), eliminating facets when they have negligible length and cells when they have negligible area. The total energy of the system is given by

$$E(t) = \sum_{\{\Gamma_i\}} \int_{\Gamma_i} \psi |b| ds \tag{2.5}$$

Owing exactly to the Herring Condition (2.3), the instantaneous rate of change of the energy

$$\begin{aligned} \frac{d}{dt} E(t) &= - \sum_{\{\Gamma_i\}} \int_{\Gamma_i} v_n^2 ds + \sum_{TJ} v \cdot \sum (\psi_\theta n + \psi b) \\ &= - \sum_{\{\Gamma_i\}} \int_{\Gamma_i} v_n^2 ds \\ &\leqq 0, \end{aligned} \tag{2.6}$$

rendering the network dissipative for the energy in any instant absent of critical events. Indeed, in an interval $(t_0, t_0 + \tau)$ where there are no critical events, we may integrate (2.6) to obtain a local dissipation equation

$$\sum_{\{\Gamma_i\}} \int_{t_0}^{t_0+\tau} \int_{\Gamma_i} v_n^2 ds dt + E(t_0 + \tau) = E(t_0) \tag{2.7}$$

which bears a strong resemblance to the simple dissipation relation for an ensemble of inertia free springs with friction. In the simulation, the facet interchange and cell deletion are arranged so that (2.6) is maintained.

Suppose, for simplicity, that the energy density is independent of the normal direction, so $\psi = \psi(\alpha)$. It is this situation that will concern us here. Then (2.2) and (2.3) may be expressed

$$v_n = \psi\kappa \text{ on } \Gamma \tag{2.8}$$

$$\sum_{i=1,\dots,3} \psi b^{(i)} = 0 \text{ at } p, \tag{2.9}$$

where p denotes a triple junction. (2.9) is the same as the Young wetting law. Our interfacial energy densities ψ are chosen so that

$$1 \leqq \psi(\alpha) \leqq \frac{3}{2}, \ |\alpha| \leqq \frac{\pi}{4}, \tag{2.10}$$

(periodic with period $\pi/2$) giving square symmetry which is intended to mimic cubic symmetry in three dimensions. For the range of ψ in (2.10), one may check that (2.9) can always be resolved, namely, given three numbers $\psi_i \in [1, 3/2]$ there are unit vectors b_i such that

$$\psi_1 b_1 + \psi_2 b_2 + \psi_3 b_3 = 0.$$

In executing this check, one may see that if the oscillation in ψ is too large, then it may not be possible to fulfill the Young Law condition in general. In practice, we have found the energy anisotropy to be less than 20%. Perhaps it is also of value to point out, in this context, that the failure of all but one cell to evacuate the network under (2.10) cannot be attributed to incompatibility but is likely due to configurational hinderance or near equilibrium behavior.

For this situation we define the grain boundary character distribution, GBCD,

$$\begin{aligned} &\rho(\alpha, t) = \text{relative length of arc of misorientation } \ \alpha \ \text{ at time } t, \\ &\text{normalized so that } \int_\Omega \rho d\alpha = 1. \end{aligned} \tag{2.11}$$

3. **Discussion of the Simulation.** The simulation of evolution is based on solving numerically the system (2.2), (2.3) for the network while managing the critical events. It must be designed so it is robust and reliable statistics can be harvested. Owing to the size and complexity of the network there are number of challenges in the designing of the method. These include

- management of the data structure of cells, facets, and triple junctions, dynamic because of critical events,
- management of the computational domain
- initialization of the computation,
- maintaining the triple junction boundary condition (2.3) while
- resolving the equations (2.2) with sufficient accuracy

We will address some of these issues below. We also need some diagnostics to understand accuracy. For example, it is known that the average area of cells grows linearly even in very casual simulations of coarsening, although more careful diagnostics show that the Herring Condition (2.3) fails. As noted in the introduction, this will lead to an unreliable determination of the GBCD.

In view of the dissipation inequality (2.6) the evolution of the grain boundary system may be viewed as a modified steepest descent for the energy. Therefore, the cornerstone of our scheme which assures its stability is the discrete dissipation inequality for the total grain boundary energy which holds when the discrete Herring Condition is satisfied.

In general, discrete dissipation principles ensure the stability and convergence of numerical schemes to the continuous solution. Here we work with a weak formulation, a variational principle, to avoid the additional complexity of higher order spaces. It is not necessary to know the normal direction, nor is there explicit use of curvature.

Let us address now some details of the more important features related to the design and implementation of the scheme. The data structure for the execution of the simulation consists of the lists of the cells - grains, edges - grain boundaries and vertices - triple junctions. These lists communicate with each other during simulation and are managed using standard linked-lists: each grain boundary has pointers to the two grains sharing it as a boundary, each boundary also has pointers to its end points, triple junctions. Each triple junction has pointers to three grain boundaries that meet at that point. Each grain has pointers to a list of its grain boundaries.

We initialize a configuration of cells and their boundary arcs, by a Voronoi diagram with N_0 seeds place randomly in the computational domain and we impose 'periodic boundary conditions' on the boundary of the domain. We would like to emphasize that we do not work with functions which have periodic boundary conditions but with cell structures which mirror each other near the borders and it must be dynamically updated. This is an important part of the algorithm and it is necessary so the statistics will always sample in the same computational domain.

Each cell is assigned an orientation and the misorientation parameter of a boundary is the difference of the orientations of the grains which share it. Typically the orientations are normally distributed, so the misorientations are also normally distributed.

The simulation of the grain network is done in three steps by evolving first the grain boundaries, according to Mullin's equation, and then updating the triple points according to Herring's boundary condition (2.3) , imposed at the triple junctions, and finally managing the rearrangement events. In our numerical simulations, grain boundaries are defined by the set of nodal points and are approximated using linear elements. In the algorithm, we define a global mesh size, h, and uniformly discretized grain boundaries with local mesh size (distance between neighboring nodal points) which depends on h. Due to the frequency of critical events, we have used a first order method in time, namely the Forward Euler method. Increasing the order of time discretization to 2 by using a predictor corrector method did not affect the distribution functions, which is the focus of this study.

Resolution of the Herring Condition: To satisfy the Herring Condition (2.3) one has to solve the nonlinear equation to determine the new position of the triple junction [41]. We use Newton's method with line search [35] to approximate the new position for the triple junction. As the initial guess for Newton's method, we determine the position of the triple point by defining the velocity of the triple junction to be proportional to the total line stress at that point with coefficient of the proportionality equal to the mobility. This is also dissipative for the network. The Newton algorithm stops if it exceeds a certain tolerance on the number of the iterations. If the Newton's algorithm converges, the Herring Condition (2.3) is satisfied with the machine precision accuracy at the new position of the triple junction. If Newton's algorithm fails to converge at some triple junctions (this happens when we work with very small cells) we use our initial guess to update its position.

Critical events: As grain growth proceeds, critical events occur. When grain boundaries (GB) shrink below a certain size, they trigger one or more of the following processes (i) short GB removal, (ii) splitting of unstable junctions (where more then three GB meet) (ii) fixing double GB (GB that share two vertices).
Removal of short GB: A short GB whose length is decreasing is removed. If its length is increasing, it is not removed.
Splitting unstable vertices: When a GB disappears, new vertices may appear where more than three edges meet. These are unstable and split, introducing a new vertex and a new GB of short length, reducing the number of edges meeting at the unstable junctions. This process continues until all vertices are triple junctions. Details of each split are designed to maximally decrease the energy.

4. **Simplified coarsening model.** A significant difficulty in developing a theory for the GBCD, and understanding texture development in general, lies in the lack of understanding of consequences of rearrangement events or critical events, facet interchange and grain deletion, on misorientations and grain size. For example, in Fig. 3, the average area of five-faceted grains during a growth experiment on an *Al* thin film and the average area of five-faceted cells in a typical simulation both increase with time. Now the von Neumann-Mullins Rule is that the area A_n of a cell with n-facets satisfies

$$A_n'(t) = c(n-6),$$

when $\psi = const.$ and hence triple junctions meet at angles of $2\pi/3$. This is thought to hold approximately when anisotropy is small. The von Neumann-Mullins Rule does not fail in the example above, of course, but cells observed at later times had 6, 7, 8, ... facets at earlier times. Thus in the network setting, changes which rearrange the network play a major role. Although we may be reasonably confident that small cells with a small number of facets will be deleted, their resulting effect on the configuration appears to be essentially random.

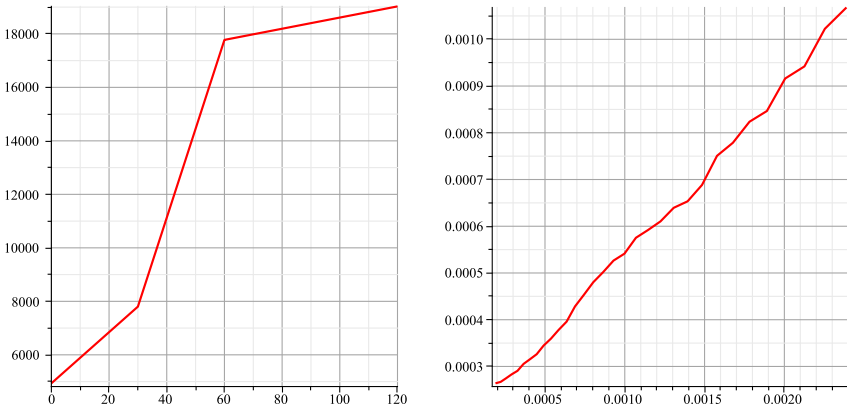

FIGURE 3. Average area of five-sided cell populations in (a) an experiment on *Al* thin film and (b) a typical simulation.

We shall approach this by a simplified model which retains kinetics and critical events but neglects curvature driven growth of the boundaries. It is an abstraction

of the role of triple junctions in the presence of the rearrangement events. We have used this model to develop a statistical theory for critical events, [12],[13],[11]. It has been found to have its own GBCD which we shall now study.

Our theme will be that the GBCD statistic for the simplified problem resembles the solution of a Fokker-Planck Equation via the mass transport implicit scheme, [37]. The first part of the discussion consists in introducing this model. The simplified model is formulated as a gradient flow which results in a dissipation inequality analogous to the one found for the coarsening grain network. Because of this simplicity, it will be possible to 'upscale' the network level system description to a higher level GBCD description that accomodates irreversibility. As this changes the ensemble, there is an entropic contribution, which we take in the form of configurational entropy. A more useful dissipation inequality is obtained by modifying the viscous term to be a mass transport term, which now brings us to the realm of the Kantorovich-Rubenstein-Wasserstein implicit scheme. This then suggests the Fokker-Planck paradigm.

The second part of the discussion, in section 5, will be our argument to validate this paradigm. We do not know the the statistic solves the Fokker-Planck PDE but we ask if it shares important aspects of Fokker-Planck behavior. We give evidence for this by asking for the unique 'temperature' parameter that minimizes the relative entropy over long time. The empirical stationary distribution and Boltzmann distribution with the special value of 'temperature' are in excellent agreement, Figure 6. This gives an explanation for the stationary distribution and the kinetics of evolution. We do not know, at this point in time, that the two dimensional network has the detailed dissipative structure of the simplified model, but we are able to produce evidence that the same argument employing the relative entropy does suggest the correct kinetics and stationary distribution.

4.1. **Formulation.** Let $I \subset \mathbf{R}$ be an interval of length L partitioned by points $x_i, i = 1, \ldots, n$, where $x_i < x_{i+1}, i = 1, \ldots, n-1$ and x_{n+1} identified with x_1. For each interval $[x_i, x_{i+1}], i = 1, \ldots, n$ select a random misorientation number $\alpha_i \in (-\pi/4, \pi/4]$. The intervals $[x_i, x_{i+1}]$ correspond to grain boundaries with misorientations α_i and the points x_i represent the triple junctions. Choose an energy density $\psi(\alpha) \geqq 0$ and introduce the energy

$$E = \sum_{i=1,\ldots,n} \psi(\alpha_i)(x_{i+1} - x_i). \tag{4.1}$$

We impose gradient flow kinetics with respect to (4.1), which is the system of ordinary differential equations

$$\begin{aligned} &\frac{dx_i}{dt} = -\frac{\partial E}{\partial x_i}, i = 1, ..., n, \text{ that is} \\ &\frac{dx_i}{dt} = \psi(\alpha_i) - \psi(\alpha_{i-1}), i = 2...n, \text{ and } \frac{dx_1}{dt} = \psi(\alpha_1) - \psi(\alpha_n). \end{aligned} \tag{4.2}$$

The velocity v_i of the i^{th} boundary is

$$v_i = \frac{dx_{i+1}}{dt} - \frac{dx_i}{dt} = \psi(\alpha_{i-1}) - 2\psi(\alpha_i) + \psi(\alpha_{i+1}). \tag{4.3}$$

The grain boundary velocities are constant until one of the boundaries collapses. That segment is removed from the list of current grain boundaries and the velocities of its two neighbors are changed due to the emergence of a new junction. Each such deletion event rearranges the network and, therefore, affects its subsequent evolution

just as in the two dimensional cellular network. Actually, since the interval velocities are constant, this gradient flow is just a sorting problem. At any time, the next deletion event occurs at smallest of

$$\frac{x_i - x_{i+1}}{v_i}.$$

The length $l_i(t)$ of the i^{th} interval is linear until it reaches 0 or until a collision event, when it becomes linear with a different slope. In any event, it is continuous, so $E(t), t > 0$, the sum of such functions multiplied by factors, is continuous.

We turn now to the dissipation inequality for the gradient flow. At any time t between deletion events,

$$\begin{aligned} \frac{dE}{dt} &= \sum \psi(\alpha_i) v_i \\ &= -\sum (\psi(\alpha_i) - \psi(\alpha_{i-1}))^2 \\ &= -\sum \frac{dx_i}{dt}^2 \leqq 0. \end{aligned} \tag{4.4}$$

Suppose that the segment $[x_c, x_{c+1}]$ is deleted at time t_c, so $v_c < 0$ for $t < t_c$ and near it. Now

$$E(t) > \sum_{i \neq c} \psi(\alpha_i) l_i(t), \text{ for } t < t_c$$

and so

$$E(t_c) = \lim_{t \to t_c^+} \sum_{i \neq c} \psi(\alpha_i) l_i(t) \leqq \lim_{t \to t_c^-} E(t)$$

Thus $E(t)$ is continuous decreasing Lipschitz (piecewise linear) with derivative given by (4.4) a.e.. We may write a mass-spring-dashpot-like local dissipation inequality analogous to the grain growth one. In an interval $(t_0, t_0 + \tau)$ where there are no critical events, dE/dt may be integrated to give

$$\tau \sum_{i=1\ldots n} \frac{dx_i}{dt}^2 + E(t_0 + \tau) = E(t_0)$$

or

$$\sum_{i=1\ldots n} \int_0^\tau \frac{dx_i}{dt}^2 dt + E(t_0 + \tau) = E(t_0) \tag{4.5}$$

With appropriate interpretation of the sum, (4.5) holds for all t_0 and almost every τ sufficiently small. With the obvious use of Young's Inequality, we have that

$$\frac{1}{4} \sum_{i=1\ldots n} \int_0^\tau v_i^2 dt + E(t_0 + \tau) \leqq E(t_0) \tag{4.6}$$

The energy of the system at time $t_0 + \tau$ is determined by its state at time t_0. Vice versa, changing the sign on the right hand side of (4.2) allows us to begin with the state at time $t_0 + \tau$ and return to the state of time t_0: the system is reversible in an interval of time absent of rearragement events. This is no longer the situation after such an event. At the later time, we have no knowledge about which interval, now no longer in the inventory, was deleted.

We introduce a new ensemble based on the misorientation parameter α where we take $\Omega : -\frac{\pi}{4} \leqq \alpha \leqq \frac{\pi}{4}$, for later ease of comparison with the two dimensional network for which we are imposing "cubic" symmetry, i.e., "square" symmetry in the plane. The $GBCD$ or character distribution in this context is, as expected,

the histogram of lengths of intervals sorted by misorientation α scaled to be a probability distribution on Ω. To be precise, let

$$\begin{aligned} l_i(\alpha,t) &= x_{i+1}(t) - x_i(t) \\ &= \text{length of the } i^{th} \text{ interval, where explicit note has been taken of} \\ &\quad \text{its misorientation parameter } \alpha \end{aligned}$$

Now partition Ω into m subintervals of length $h = \frac{\pi}{2}\frac{1}{m}$ and let

$$\rho(\alpha,t) = \sum_{\alpha' \in ((k-1)h,kh]} l_i(\alpha',t) \cdot \frac{1}{Lh}, \text{ for } (k-1)h < \alpha \leqq kh. \tag{4.7}$$

For this definition of the statistic,

$$\int_\Omega \rho(\alpha,t) d\alpha = 1$$

Let us make a reasonable estimate of

$$\frac{\partial \rho}{\partial t}(\alpha,t) = \sum_{\alpha' \in ((k-1)h,kh]} v_i(\alpha') \cdot \frac{1}{Lh}, \text{ for } (k-1)h < \alpha \leqq kh. \tag{4.8}$$

Generally speaking suppose that there are M data points in the sample and that this number is approximately the same throughout the simulation and they are uniformly distributed in the m bins. The approximate number of items of data in each box is given by

$$\sharp\{l(\alpha',t)\} = M \cdot \frac{1}{m} = \frac{2}{\pi} \cdot Mh$$

Hence, using Schwarz, as more or less a good guess,

$$\begin{aligned} |\frac{\partial \rho}{\partial t}(\alpha,t)|^2 &\leqq (\frac{1}{Lh})^2 \sum_{\alpha' \in ((k-1)h,kh]} v_i^2 \cdot \sharp\{l(\alpha',t)\} \\ &= \frac{2M}{\pi L^2} \sum_{\alpha' \in ((k-1)h,kh]} v_i^2 \frac{1}{h}, \text{ for } (k-1)h < \alpha \leqq kh, \end{aligned}$$

whence integrating over Ω, that is summing over all the intervals $((k-1)h, kh]$, $k = 1, \ldots, m$,

$$\begin{aligned} \int_\Omega |\frac{\partial \rho}{\partial t}(\alpha,t)|^2 d\alpha &\leqq \sum_{k=1,\ldots,m} \frac{2M}{\pi L^2} \sum_{\alpha' \in ((k-1)h,kh]} v_i^2 \frac{1}{h} \cdot h, \\ &\leqq \frac{2M}{\pi L^2} \sum_i v_i^2 \end{aligned} \tag{4.9}$$

The right hand side of $(4.9)_2$ is bounded in terms of initial parameters.

Note that

$$E(t) = \sum \psi(\alpha_i) \cdot \frac{1}{Lh} l_i(\alpha_i,t) \cdot Lh = L \int_\Omega \psi(\alpha)\rho(\alpha,t) d\alpha,$$

where an $O(h)$ term has been neglected.

We may express (4.6) in terms of the character distribution (4.7), which amounts to

$$\mu_0 \int_{t_0}^{t_0+\tau} \int_\Omega |\frac{\partial \rho}{\partial t}(\alpha,t)|^2 d\alpha dt + \int_\Omega \psi(\alpha)\rho(\alpha,t_0+\tau) d\alpha \leqq \int_\Omega \psi(\alpha)\rho(\alpha,t_0) d\alpha, \tag{4.10}$$

where $\mu_0 > 0$ is some constant.

We now impose a modeling assumption. The expression (4.10) is in terms of the new misorientation level ensemble, upscaled from the local level of the original system, and, consistent with the lack of reversibility when rearrangement events occur, an entropic term will be added. We use standard configurational entropy,

$$+\int_\Omega \rho\log\rho d\alpha, \tag{4.11}$$

although this is not the only choice. Minimizing (4.11) favors the uniform state, which would be the situation were $\psi(\alpha) = \text{constant}$.

Given that (4.10) holds, we assume that for any t_0 and τ sufficiently small that

$$\mu_0\int_{t_0}^{t_0+\tau}\int_\Omega (\frac{\partial\rho}{\partial t})^2 d\alpha dt + \int_\Omega (\psi\rho+\lambda\rho\log\rho)d\alpha|_{t_0+\tau} \leqq \int_\Omega (\psi\rho+\lambda\rho\log\rho)d\alpha|_{t_0} \tag{4.12}$$

$E(t)$ was analogous to an internal energy or the energy of a microcanonical ensemble and now

$$F(\rho) = F_\lambda(\rho) = E(t) + \lambda\int_\Omega \rho\log\rho d\alpha \tag{4.13}$$

is a free energy.

4.2. **Mass transport paradigm.** Let us first briefly review the notion of Kantorovich-Rubenstein-Wasserstein metric, or simply Wasserstein metric, and some known results that will be used in our analysis below. The reader can consult [59], [3] for more detailed exposition of the subject.

Let $D \subset \mathbf{R}$ be an interval, perhaps infinite, and f^*, f a pair of probability densities on D (with finite variance). The quadratic Wasserstein metric or 2-Wasserstein metric is defined to be

$$\begin{aligned} &d(f,f^*)^2 = \inf_P \int_D |x-y|^2 dp(x,y) \\ &P = \text{joint distributions for } f, f^* \text{ on } \bar{D}\times\bar{D}, \end{aligned} \tag{4.14}$$

i.e., the marginals of any $p \in P$ are f, f^*. The metric induces the weak-$*$ topology on $C(\bar{D})'$. If f, f^* are strictly positive, there is a transfer map which realizes p, essentially the solution of the Monge-Kantorovich mass transfer problem for this situation. This means that there is a strictly increasing

$$\begin{aligned} &\phi : D \to D \text{ such that} \\ &\int_D \zeta(y)f(y)dy = \int_D \zeta(\phi(x))f^*(x)dx,\ \zeta \in\ C(\bar{D}),\ \text{and} \\ &d(f,f^*)^2 = \int_D |x-\phi(x)|^2 f^* dx \end{aligned} \tag{4.15}$$

In this one dimensional situation, as was known to Frechét, [24],

$$\begin{aligned} &\phi(x) = F^{*-1}(F(x)),\ x\in D, \text{where} \\ &F^*(x) = \int_{-\infty}^x f^*(x')dx' \text{ and } F(x) = \int_{-\infty}^x f(x')dx' \end{aligned} \tag{4.16}$$

are the distribution functions of f^*, f. In one dimension there is only one transfer map. Finally, by a result of Benamou and Brenier [15],

$$\begin{aligned}&\frac{1}{\tau}d(f,f^*)^2 = \inf \int_0^\tau \int_D v^2 f d\xi dt\\ &\text{over deformation paths } f(\xi,t) \text{ subject to}\\ &f_t + (vf)_\xi = 0, \text{ (continuity equation)}\\ &f(\xi,0) = f^*(\xi), f(\xi,\tau) = f(\xi) \text{ (initial and terminal conditions)}\end{aligned} \tag{4.17}$$

The conditions (4.17) are in 'Eulerian' form. Likewise there is the 'Lagrangian' form which follows by rewriting (4.17) using the transfer function formulation in (4.15),

$$\begin{aligned}&\frac{1}{\tau}d(f,f^*)^2 = \inf \int_0^\tau \int_D \phi_t^2 f^* dx\\ &\text{over transfer paths } \phi(x,t) \text{ from } D \text{ to } D \text{ with}\\ &\phi(x,0) = x \text{ and } \phi(x,\tau) = \phi(x)\end{aligned} \tag{4.18}$$

Now let us go back and consider the inequality (4.12) above. This energy inequality fails as a proper dissipation principle because the first term

$$\mu_0 \int_{t_0}^{t_0+\tau} \int_\Omega (\frac{\partial \rho}{\partial t})^2 d\alpha dt$$

does not represent lost energy due to frictional or viscous forces. For a deformation path $f(\alpha,t), t_0 \leqq t \leqq t_0+\tau$, of probability densities, this quantity is

$$\int_0^\tau \int_\Omega v^2 f d\alpha dt \tag{4.19}$$

where f, v are related by the continuity equation and initial and terminal conditions

$$\begin{aligned}&f_t + (vf)_\alpha = 0 \text{ in } \Omega \times (t_0, t_0+\tau), \text{and}\\ &f(\alpha,t_0) = \rho(\alpha,t_0),\ f(\alpha,t_0+\tau) = \rho(\alpha,t_0+\tau),\end{aligned} \tag{4.20}$$

by analogy with fluids [43], p.53 et seq., and elementary mechanics.
Therefore, our goal is to replace the expression (here we denote the starting time t_0 by 0)

$$\int_0^\tau \int_\Omega (\frac{\partial \rho}{\partial t})^2 d\alpha dt \tag{4.21}$$

in (4.5) or (4.13) by a proper dissipation term, eg. (4.19) and subseqently by the Wasserstein metric introduced above. Since they induce different topologies on probability densities, an inequality where (4.21) dominates (4.14) will involve terms other than the two metrics themselves.

Let us proceed as follows. Let Ω be a bounded interval, say $\Omega = (0,1)$. Assume that our statistic $\rho(\alpha,t)$ satisfies

$$\rho(\alpha,t) \geqq \delta > 0 \text{ in } \Omega, t > 0. \tag{4.22}$$

This is a necessary assuption for our estimates below. In fact, to proceed with the implicit scheme introduced later, it is sufficient to require (4.22) just for the initial data $\rho_0(\alpha)$ since this property is inherited by the iterates. We now use the

representation (4.17) and we use the deformation path given by ρ itself to calculate that for some $c_\Omega > 0$,

$$\begin{aligned} &\frac{1}{\tau} d(\rho, \rho^*)^2 \leqq \int_0^\tau \int_\Omega v^2 \rho dx dt \leqq \frac{c_\Omega}{\min_\Omega \rho} \int_0^\tau \int_\Omega \frac{\partial \rho}{\partial t}(x,t)^2 dx dt, \\ &\rho^*(x) = \rho(x,0) \text{ and } \rho(x) = \rho(x,\tau), \end{aligned} \tag{4.23}$$

where 0 represents an arbitrary starting time and τ a relaxation time. Given the pair (v, ρ), integrate the continuity equation in (4.17) to obtain the non-conservative form

$$\frac{\partial F}{\partial t} + v \frac{\partial F}{\partial x} = \frac{\partial F}{\partial t} + v\rho = c \text{ in } \Omega, 0 < t < \tau.$$

Now $F_t|_{\partial\Omega} = 0$ and $v|_{\partial\Omega} = 0$ for $0 < t < \tau$, so the possibly time dependent constant above vanishes. Thus

$$v^2 \rho(x,t) = \frac{F_t(x,t)^2}{\rho(x,t)} \leqq \frac{x}{\rho(x,t)} \int_\Omega \rho_t(y,t)^2 dy, \;\; x \in \Omega, 0 < t < \tau \tag{4.24}$$

Integrating (4.24),

$$\begin{aligned} \int_0^\tau \int_\Omega v^2 \rho dx dt &\leqq \int_0^\tau \int_\Omega \frac{x}{\rho(x,t)} dx \int_\Omega \rho_t(y,t)^2 dy dt \\ &\leqq \frac{c_\Omega}{\min_\Omega \rho} \cdot \int_0^\tau \int_\Omega \rho_t(y,t)^2 dy dt. \end{aligned} \tag{4.25}$$

Thus, again keeping (4.17) in mind,

$$\frac{1}{\tau} d(\rho, \rho^*)^2 = \inf \int_0^\tau \int_\Omega v^2 \rho d\xi dt \leqq \frac{c_\Omega}{\min_\Omega \rho} \cdot \int_0^\tau \int_\Omega \rho_t(y,t)^2 dy dt. \tag{4.26}$$

Hence, in view of (4.26), we obtain (4.23).

We then find that there is a $\mu > 0$ such that for any relaxation time $\tau > 0$,

$$\frac{\mu}{2} \int_0^\tau \int_\Omega v^2 \rho d\alpha dt + F_\lambda(\rho) \leqq F_\lambda(\rho^*) \tag{4.27}$$

We next replace (4.27) by a minimum principle, arguing that the path given by $\rho(\alpha, t)$ is the one most likely to occur and the minimizing path has the highest probability. For this step, let $\rho^* = \rho(\cdot, t_0)$ and $\rho = \rho(\cdot, t + \tau)$. Observe that from (4.17),

$$\begin{aligned} &\frac{1}{\tau} d(\rho, \rho^*)^2 = \inf \int_0^\tau \int_\Omega v^2 f d\alpha dt \\ &\text{over deformation paths } f(\alpha, t) \text{ subject to} \\ &f_t + (vf)_\alpha = 0, \text{ (continuity equation)} \\ &f(\xi, 0) = \rho^*(\alpha), f(\alpha, \tau) = \rho(\alpha, \tau) \text{ (initial and terminal conditions)} \end{aligned} \tag{4.28}$$

where d is the Wasserstein metric. So we may express the minimum principle in the form

$$\frac{\mu}{2\tau} d(\rho, \rho^*)^2 + F_\lambda(\rho) = \inf\{\frac{\mu}{2\tau} d(\eta, \rho^*)^2 + F_\lambda(\eta)\} \tag{4.29}$$

For each relaxation time $\tau > 0$ we determine iteratively the sequence $\{\rho^{(k)}\}$ by choosing $\rho^* = \rho^{(k-1)}$ and $\rho^{(k)} = \rho$ in (4.29) and set

$$\rho^{(\tau)}(\alpha, t) = \rho^{(k)}(\alpha) \text{ in } \Omega \text{ for } k\tau \leqq t < (k+1)\tau. \tag{4.30}$$

We then anticipate recovering the GBCD ρ as

$$\rho(\alpha,t)=\lim_{\tau\to 0}\rho^{(\tau)}(\alpha,t), \tag{4.31}$$

with the limit taken in a suitable sense. It is known for some time that ρ obtained from (4.31) is the solution of the Fokker-Planck Equation, [37] or see Appendix 8.1 for the brief description.

$$\mu\frac{\partial\rho}{\partial t}=\frac{\partial}{\partial\alpha}(\lambda\frac{\partial\rho}{\partial\alpha}+\psi'\rho) \text{ in } \Omega, 0<t<\infty. \tag{4.32}$$

We might point out here, as well, that a solution of (4.32) with periodic boundary conditions and nonnegative initial data is positive for $t>0$.

5. **Validation of the scheme.** We now begin the validation step of our model. Introduce the notation for the Boltzmann distribution with parameter λ

$$\rho_\lambda(\alpha)=\frac{1}{Z_\lambda}e^{-\frac{\psi(\alpha)}{\lambda}}, \alpha\in\Omega, \text{ with } Z_\lambda=\int_\Omega e^{-\frac{\psi(\alpha)}{\lambda}}d\alpha. \tag{5.1}$$

As outlined in Appendix 8.2, with validation we would gain qualitative properties of solutions of (4.32):

- $\rho(\alpha,t)\to\rho_\lambda(\alpha)$ as $t\to\infty$, and
- this convergence is exponentially fast.

The Kullback-Leibler relative entropy for (4.32) is given by

$$\begin{aligned}&\Phi_\lambda(\eta)=\lambda\int_\Omega\eta\log\frac{\eta}{\rho_\lambda}d\alpha \text{ where}\\ &\eta\geqq 0 \text{ in } \Omega, \int_\Omega\eta d\alpha=1,\end{aligned} \tag{5.2}$$

with ρ_λ from (5.1). By Jensen's Inequality it is always nonnegative. In terms of the free energy (4.13) and (5.1), (5.2) is given by

$$\Phi_\lambda(\eta)=F_\lambda(\eta)+\lambda\log Z_\lambda. \tag{5.3}$$

The procedure which leads to the implicit scheme, based on the dissipation inequality (4.6), holds for the entire system but does not identify individual intermediate 'spring-mass-dashpots'. The consequence is that we cannot set the temperature-like parameter σ, but in some way must decide if one exists. Therefore, we seek to identify the particular $\lambda=\sigma$ for which Φ_σ defined by the GBCD statistic ρ tends monotonely to the minimum of all the $\{\Phi_\lambda\}$ as t becomes large. We then ask if the terminal, or equilibrium, empirical distribution ρ is equal to ρ_σ. For our purposes, we simply decide the question of equality by inspection.

In this context, deciding a parameter on the basis of its thermodynamic restrictions is employed in [17],[18],[19] and recalls the Coleman-Noll procedure.

To understand our implementation, we offer an illustration using the solution of the (4.32) itself, u computed on $\Omega=(0,1)$ with the choice $\lambda=\sigma=0.0296915$, and a collection of relative entropy plots $\{\Phi_\lambda\}$ where values of λ are close to σ, cf. Figure 4(left). The plot of Φ_σ vs. time t is noted in red and it is decreasing and tends to 0. A glance at the resulting equilibrium u, Figure 4(right), identifies it as the Boltzmann distribution ρ_σ, as constructed.

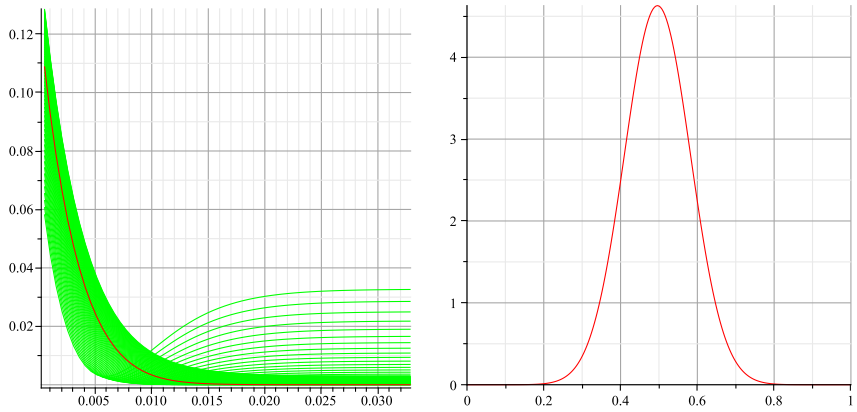

FIGURE 4. (left) The relative entropy Φ_σ of the solution $u(x,t)$ of the Fokker-Planck Equation (4.32) for the potential $\psi(x) = 1 + r(x - \frac{1}{2})^2, r = 2$, with the choice $\lambda = \sigma = 0.0296915$, computed by a routine numerical method, compared with a sequence of Φ_λ with the curve for $\sigma = 0.0296915$ noted in red. The values of λ correspond to ρ_λ with $\max \rho_\sigma/2 \leqq \max \rho_\lambda \leqq (3/2) \max \rho_\sigma$ (right) The computed equlibrium solution, which is indistinguishable from ρ_σ, the Boltzmann distribution of (5.2).

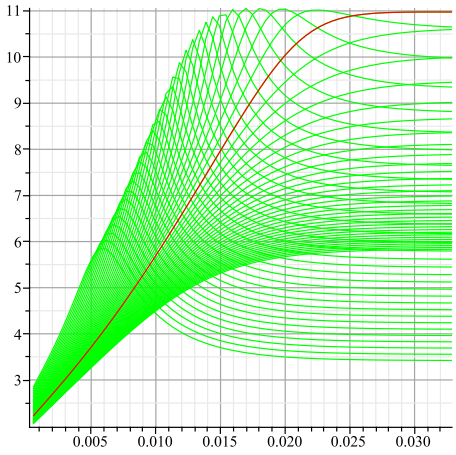

FIGURE 5. Plots of $-\log \Phi_\lambda$ vs. t with $-\log \Phi_\sigma$ in red. Plot illustrates that Φ_σ decreases exponentially to 0 but that Φ_λ for choices of $\lambda \neq \sigma$ do not have this property.

For the simplified coarsening model, we consider

$$\psi(\alpha) = 1 + 2\alpha^2 \text{ in } \Omega = (-\frac{\pi}{4}, \frac{\pi}{4}), \tag{5.4}$$

and shall identify a unique such parameter, which we label σ, by seeking the minimum of the relative entropy (5.2) and then comparing it with ρ_σ. This ψ the development to second order of $\psi(\alpha) = 1 + 0.5 \sin^2 2\alpha$ used in the 2D simulation. Moreover, since the potential is quadratic, it represents a version of the Ornstein-Uhlenbeck process. To proceed, we must agree upon which time T_∞ represents time

equals infinity. For the simplified critical event model we are considering, it is clear that by computing for a sufficiently long time, all cells will be gone. This time may be quite long. We choose the time parameter so that 80% of segments have been deleted, which corresponds to the stationary configuration in the two-dimensional simulation. For the simplifed model simulation, this time is $T(80\%) = 6.73$. For comparison, $T(90\%) = 30$ and $T(95\%) = 103$. There may be additional criteria for choosing a T in the neighborhood of $T(80\%)$ and we may wish to discuss this later.

This simulation is initialized with $2^{15} + 1$ cells and approximately 155 trial distributions ρ_j are collected at 200 rearrangement event intervals. 155 trial relative entropies are constructed from gaussians ρ_{λ_j} satisfying

$$\rho_{\lambda_j}(0) = \max \rho_{\lambda_j} = \max \rho_j. \tag{5.5}$$

A selection of these are shown in Figure 6. We include the collection of plots of

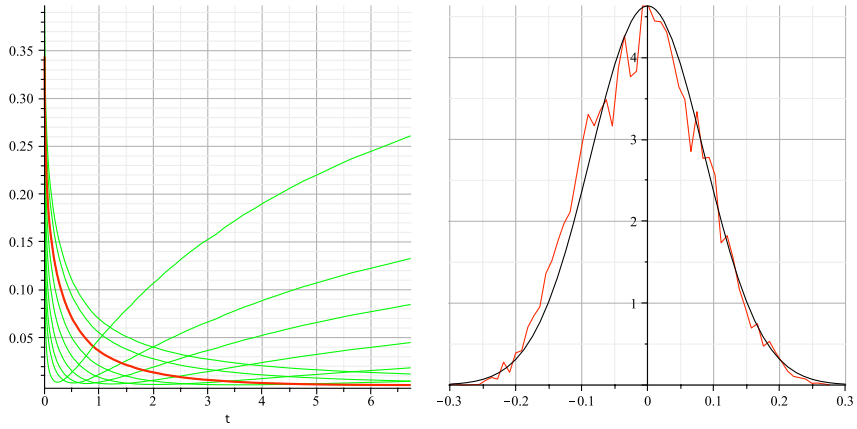

FIGURE 6. Graphical results for the simplified coarsening model. (left) Relative entropy plots for values of λ chosen according to (5.5) with Φ_σ noted in red. The value of $\sigma = 0.0296915$. (right) Empirical distribution at time $T = T_\infty$ in red compared with ρ_σ in black.

$\log \Phi_\lambda$ which suggests that Φ_σ decays exponentially to its minimum whereas a Φ_λ corresponding to a subsequent empirical distribution does not.

For a second example to illustrate the method, we consider the potential

$$\psi(\alpha) = 1 + \epsilon\alpha^4, \ -\frac{\pi}{4} \leqq \alpha \leqq \frac{\pi}{4}, \ \epsilon = 8. \tag{5.6}$$

This choice, $\epsilon = 8$, corresponds to the first order terms in the two dimensional quartic energy density we discuss in the next section.

6. **The entropy method for the GBCD.** We shall apply the method of Section 5 to the GBCD harvested from the 2D simulation. We consider first a typical simulation with the energy density

$$\psi(\alpha) = 1 + \epsilon(\sin 2\alpha)^2, \ -\frac{\pi}{4} \leqq \alpha \leqq \frac{\pi}{4}, \ \epsilon = 1/2, \tag{6.1}$$

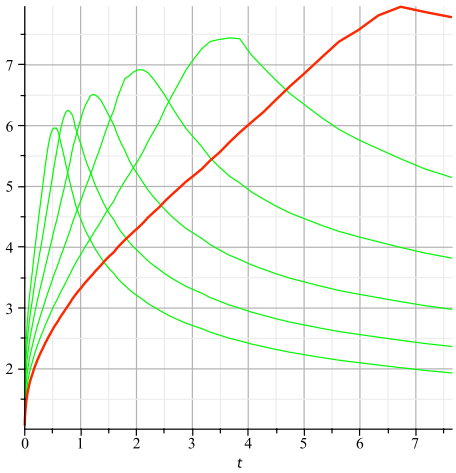

FIGURE 7. Plots of $-\log \Phi_\lambda$ vs. t with $-\log \Phi_\sigma, \sigma = 0.0296915$, in red for the simplified coarsening model. It shows that Φ_σ decays exponentially to its minimum at time T_∞. Φ_λ with $\lambda = 0.01375688608$ in black does not seem to have this property of exponential decay.

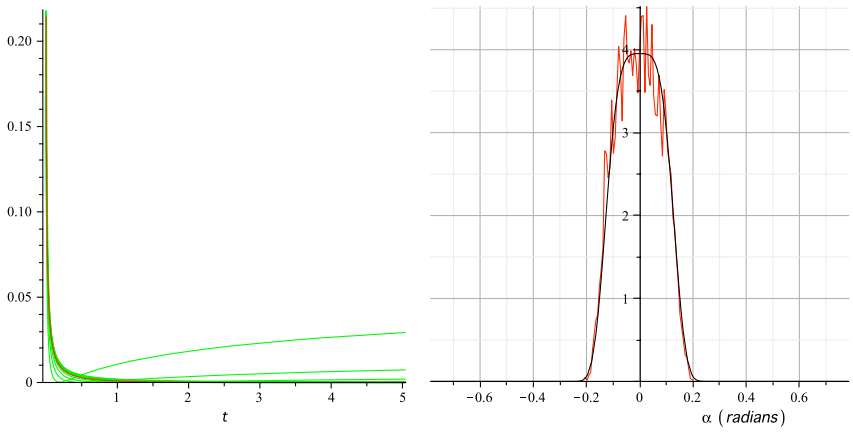

FIGURE 8. Graphical results for the simplfied coarsening model with potential (5.6). (left) Relative entropy plot for selected values of λ with Φ_σ noted in red. The value of $\sigma = 0.003033356683$ and is ascertained at the time $T = T_\infty$ corresponding to 80% of cells deleted. (right) Empirical distribution at time $T = T_\infty$ in red compared with ρ_σ in black.

Figure 9, initialized with 10^4 cells and normally distributed misorientation angles and terminated when 2000 cells remain. At this stage, the simulation is essentially stagnant. Possible 'temperature' parameters λ are constructed similarly to those of the simplified coarsening model. From the maximum of a harvested GBCD, we construct the gaussian with the same maximum. This determines a value of λ which is used to define ρ_λ in (5.1) for the density (6.1). This ρ_λ then defines a trial relative entropy via (5.2).

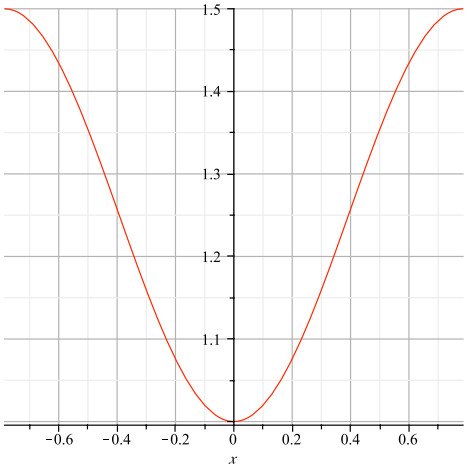

FIGURE 9. The energy density $\psi(\alpha) = 1 + \epsilon \sin^2 2\alpha,\ |\alpha| < \pi/4,\ \epsilon = \frac{1}{2}$.

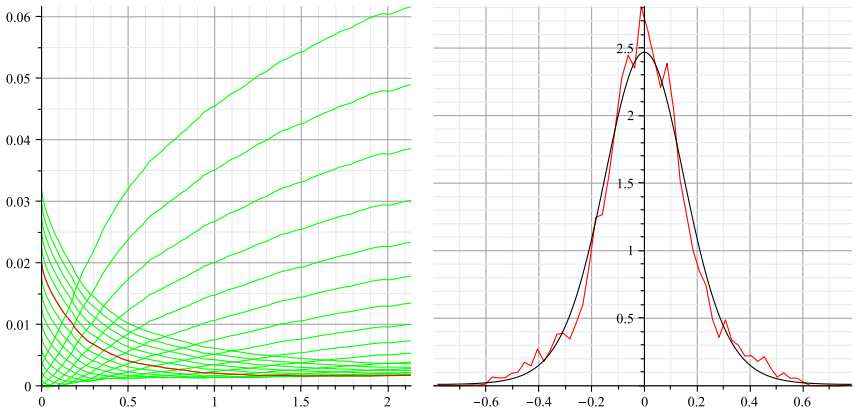

FIGURE 10. (a) The relative entropy of the grain growth simulation with energy density (6.1) for a sequence of Φ_λ vs. t with the optimal choice $\sigma \approx 0.1$ noted in red. (b) Comparison of the empirical distribution at time $t = 2$, when 80% of the cells have been deleted, with ρ_σ, the Boltzmann distribution of (5.1).

We now identify the parameter σ, which turns out to be $\sigma \approx 0.1$, Figure 10. From Figure 11, we see that this relative entropy Φ_σ has exponential decay until it reaches a value of about 1.5, when it remains constant. The solution itself then tends exponentially in L^1 to its limit ρ_σ by the Kullback-Leibler Inequality.

A second example presented here is a quartic energy

$$\psi(\alpha) = 1 + \epsilon(\sin 2\alpha)^4,\ -\frac{\pi}{4} \leqq \alpha \leqq \frac{\pi}{4},\ \epsilon = 1/2. \tag{6.2}$$

Again, a configuration of 10^4 cells is initialized with normally distributed misorientations and, this time, the computation proceeds until about 1000 cells remain.

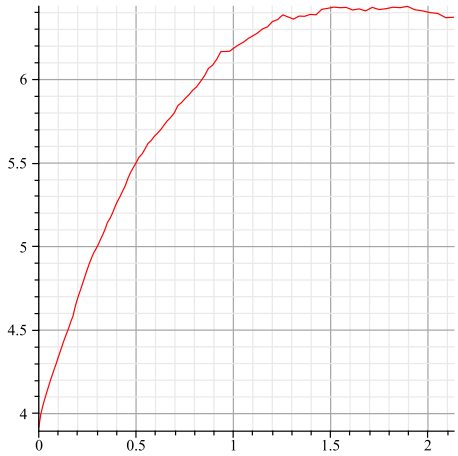

FIGURE 11. Plot of $-\log \Phi_\sigma$ vs. t with energy density (6.1). It is approximately linear until it becomes constant showing that Φ_σ decays exponentially

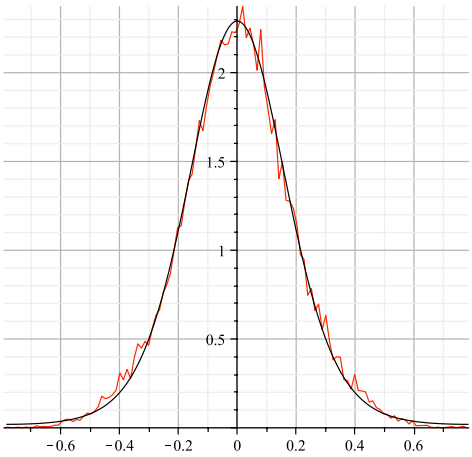

FIGURE 12. GBCD (red) and Boltzmann distribution (black) for the potential ψ of (6.1) with parameter $\sigma \approx 0.1$ as predicted by our theory. This GBCD is averaged over 5 trials.

The relative entropy and the equilibrium Boltzmann statistic stabilize when 2000 cells remain.

With the equilibrium solution in hand, as depicted in Figure 13, we again initialized a configuration of 10^4 cells with, on this occasion, misorientations normally distributed in the much narrower range defined by the sides of the solution GBCD. Since these misorientations see, essentially, only the near minimum of the potential, we would expect the new stationary distribution to be gaussian or random. However we obtain the same relative entropy curve and equilibrium depicted in Figure 13. Although this is not like a molecular system with eternal collisions causing the entire system to equilibrate, the fluctuations of misorientations caused by the

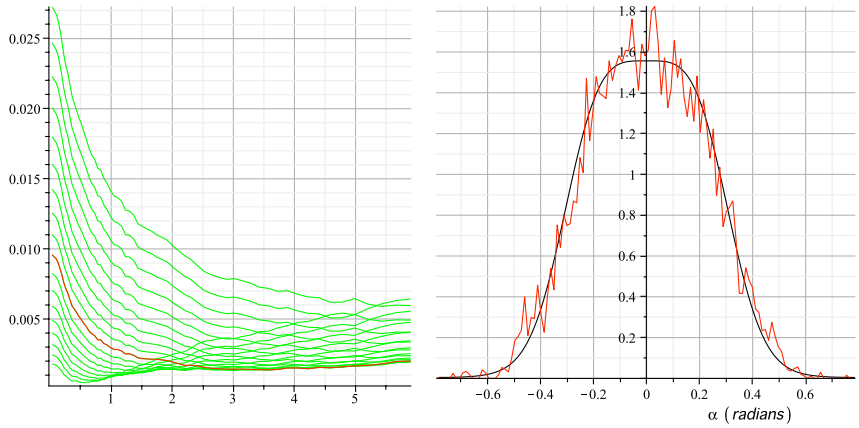

FIGURE 13. (a) The relative entropy of the grain growth simulation with density (6.2) for a sequence of Φ_λ vs. t with the optimal choice $\sigma \approx 0.08$ noted in red. (b) Comparison of the empirical distribution at time $t = 2$, when 80% of the cells have been deleted, with ρ_σ, the Boltzmann distribution of (5.1).

'perpetual' critical events provide the system with a sufficiently ample library to be driven by the given grain boundary energy density. On the other hand, we may defeat this attribute, for example, with a Read-Shockley type of energy, which is cusp-like near the origin and rises sharply to a maximum. Although near the origin, we obtain a reasonable distribution, there are otherwise insufficent orientations to populate a Boltzmann distribution, [8].

Future work will address the theory when the interfacial energy density $\psi = \psi(\theta, \alpha)$ depends on both normal angle and misorientation of the interface. In this context, we have observed that simply resolving the solution of the Fokker-Planck Equation with quartic potential leads to bimodal intermediate distributions, which are the stationary distributions for quartic interfacial energy distributions. [55, 40] This suggests that this situation represents the quenched solution of a Fokker Planck Equation and a role for the second eigenfunction of the equation. Other effects will also be studied. These can be added to the local evolution law, most simply, varying mobility, and other retarding forces such as triple junction drag.

7. **Discussion/conclusions.** Here we have outlined an entropy based theory of the GBCD which is an upscaling of cell growth according to the two most basic properties of a coarsening network: a local evolution law and space filling constraints. The theory accomodates the irreversibility conferred by the critical events or topological rearrangements which arise during coarsening. Details are given for a model system where the analytical tools are easily exploited and is seen to describe well the results of two dimensional simulations. Our principal conclusion is that these events occur preferentially in a manner that renders the GBCD closely related to the solution of a Fokker Planck Equation whose potential is the given interfacial energy density. This reasoning exploits the recent characterization of Fokker-Planck kinetics as a gradient flow for the free energy.

We note that the theory states in particular that it is the GBCD that is a consequence of the coarsening process. The traditional texture distribution is the orientation distribution (OD), the distribution of grain orientations. The GBCD

is the distribution of differences of the OD, basically the convolution of the OD with itself. This relationship may be inverted, by elementary Fourier analysis, so, in this simple case, the GBCD determines the OD and not the other way around. Therefore, we may expect, in nature, that it is among the processes that determine the OD.

8. Appendix: The Kantorovich-Rubinstein-Wasserstein (KRW) implicit scheme for Fokker-Planck Equation and the asymptotic behavior.

8.1. **The KRW implicit scheme for the Fokker-Planck Equation.** The Fokker-Planck Equation is the Euler-Lagrange Equation of a gradient flow for a free energy with respect to the Wasserstein metric, [37], as is now well established. Here we give a very brief description. Give a (smooth) potential ψ and a parameter $\sigma > 0$ defined on a bounded interval Ω, for definiteness, and define the free energy defined on probability densities

$$F(\rho) = \int_\Omega (\psi\rho + \sigma\rho\log\rho)dx. \tag{8.1}$$

Given initial data ρ_0 and $\tau > 0$, a relaxation time, we iteratively determine a sequence $\{\rho^{(k)}\}$ with the procedure: set $\rho^{(0)} = \rho_0$ and given $\rho^* = \rho^{(k-1)}$ determine $\rho^{(k)} = \rho$ the solution of the variational problem

$$\begin{aligned}&\frac{1}{2\tau}d(\rho,\rho^*)^2 + F(\rho) = \inf_{\{\eta\}}\{\frac{1}{2\tau}d(\eta,\rho^*)^2 + F(\eta)\},\\ &\{\eta\} = \text{probability densities on } \Omega \text{ subject to appropriate boundary conditions.}\end{aligned} \tag{8.2}$$

Setting

$$\rho^{(\tau)}(x,t) = \rho^{(k)}(x) \text{ for } k\tau \leqq t < (k+1)\tau, \tag{8.3}$$

the limit function

$$\rho = \lim_{\tau\to 0}\rho^{(\tau)}$$

satisfies the Fokker-Planck Equation

$$\frac{\partial\rho}{\partial t} = \frac{\partial}{\partial x}(\sigma\frac{\partial\rho}{\partial x} + \psi'\rho),\ x\in\Omega, t>0, \tag{8.4}$$

along with the appropriate boundary conditions, natural or periodic, and initial condition $\rho = \rho_0$.

A known property of the iteration procedure in (8.2) is that iterates remain positive, indeed, bounded below, if the initial data is positive and are bounded above. This simplifies the limiting process.

8.2. **Asymptotic behavior.** One of the diagnostics we consider in the analysis of the GBCD and the one we employ to identify the 'temperature' parameter σ is the decay of the relative entropy. It is straightforward to show that the relative entropy tends to zero as $t\to\infty$, and we review it below. The decay is also exponential. This is not surprising since the same is true for convergence to the stationary state for a finite ergodic Markov chain. There are many ways to show this for (8.4). It follows from the Sturm-Liouville theory and separation of variables, [25] or the Krein-Rutman theorem. A more recent technique is to use a log-Sobolev inequality. Here we sketch an inexpensive version based on an energy estimate which does not actually require the log-Sobolev inequality.

Let us assume throughout that $\rho(x,t)$ is a solution of (8.4) in Ω, a bounded interval, namely

$$\begin{aligned} &\frac{\partial \rho}{\partial t} = \frac{\partial}{\partial x}(\sigma \frac{\partial \rho}{\partial x} + \psi' \rho),\ x \in \Omega, t > 0, \\ &\sigma \frac{\partial \rho}{\partial x} + \psi' \rho = 0 \text{ on } \partial\Omega, t > 0, \end{aligned} \tag{8.5}$$

or

$$\begin{aligned} &\frac{\partial \rho}{\partial t} = \frac{\partial}{\partial x}(\sigma \frac{\partial \rho}{\partial x} + \psi' \rho),\ x \in \Omega, t > 0, \\ &\rho \text{ periodic in } x \text{ for } t > 0. \end{aligned} \tag{8.6}$$

First we establish the adjoint equation. Let

$$\rho^\sharp(x) = \frac{1}{Z} e^{-\frac{\psi(x)}{\sigma}},\ x \in \Omega, \text{ with } Z = \int_\Omega e^{-\frac{\psi(x)}{\sigma}} dx, \tag{8.7}$$

denote the stationary distribution for (8.5) or (8.6) For a smooth ζ,

$$\begin{aligned} \int_\Omega \rho_t \zeta dx &= \int_\Omega (\sigma \rho_x + \psi' \rho)_x \zeta dx \\ &= -\int_\Omega (\sigma \rho_x + \psi' \rho) \zeta_x dx \\ &= -\sigma \int_\Omega (\rho_x + \frac{\psi'}{\sigma} \rho) \zeta_x dx \\ &= -\sigma \int_\Omega e^{-\frac{\psi}{\sigma}} (e^{\frac{\psi}{\sigma}} \rho)_x \zeta_x dx \end{aligned} \tag{8.8}$$

Rewriting (8.8), we have that

$$\int_\Omega (\frac{\rho}{\rho^\sharp})_t \zeta \rho^\sharp dx = -\sigma \int_\Omega (\frac{\rho}{\rho^\sharp})_x \zeta_x \rho^\sharp dx. \tag{8.9}$$

So

$$u(x,t) = (\frac{\rho}{\rho^\sharp})(x,t),\ a(x) = \rho^\sharp(x),\ x \in \Omega,\ t > 0$$

satisfies

$$a u_t = \sigma (a u_x)_x,\ x \in \Omega,\ t > 0. \tag{8.10}$$

Let $\varphi(\xi)$ be convex, nonnegative, and consider

$$\Phi(t) = \int_\Omega \varphi(\frac{\rho}{\rho^\sharp}) \rho^\sharp dx = \int_\Omega \varphi(u) a dx \tag{8.11}$$

and compute its derivative. We have that

$$\begin{aligned} \Phi'(t) &= \frac{d}{dt} \int_\Omega \varphi(u) a dx \\ &= \int_\Omega \varphi'(u) a u_t dx \\ &= \sigma \int_\Omega \varphi'(u) (a u_x)_x dx \\ &= -\sigma \int_\Omega \varphi''(u) u_x^2 a dx < 0. \end{aligned} \tag{8.12}$$

Thus Φ is decreasing and

$$\Phi(0) - \Phi(\infty) = \sigma \int_0^\infty \int_\Omega \varphi''(u) u_x^2 a dx dt < +\infty$$

Since $\varphi'' \geqq 0$ and a is bounded below, it follows that

$$\int_\Omega \varphi''(u) u_x^2 a dx \to 0 \text{ as } t \to \infty. \tag{8.13}$$

Choose, for example,

$$\varphi(\xi) = \frac{1}{2}(\xi - 1)^2. \tag{8.14}$$

Then we deduce that

$$\begin{aligned} &\int_\Omega u_x^2 a dx \to 0 \text{ as } t \to \infty, \text{ so} \\ &u \to \textit{constant} = 1 \text{ as } t \to \infty. \end{aligned} \tag{8.15}$$

This means that, up to a subsequence,

$$\begin{aligned} &\rho(x,t) \to \rho^\sharp(x) \text{ as } t \to \infty \quad \text{and} \\ &\Phi(t) \to \varphi(1) \text{ as } t \to \infty \end{aligned} \tag{8.16}$$

In particular, whenever $\varphi(1) = 0$, we have that $\Phi(\infty) = 0$, which holds in particular for (8.14) and for the relative entropy, in this form given by

$$\varphi(\xi) = \xi \log \xi. \tag{8.17}$$

Our concern is the rate at which the relative entropy

$$\Phi(t) = \sigma \int_\Omega u \log u \; a dx = \int_\Omega \rho \log \frac{\rho}{\rho^\sharp} dx \tag{8.18}$$

tends to 0.

First note the Poincaré-style inequality: For $\zeta \in H^1(\Omega)$ with

$$\begin{aligned} &\int_\Omega \zeta a dx = 0, \\ &\text{we have that} \\ &\int_\Omega \zeta^2 a dx \leqq C_0 \int_\Omega \zeta_x^2 a dx \end{aligned} \tag{8.19}$$

Now look at

$$U(t) = \frac{1}{2}\int_\Omega (u-1)^2 a dx \text{ for which } \int_\Omega (u-1) a dx = 0. \tag{8.20}$$

Using (8.12) and (8.19),

$$\begin{aligned} \frac{dU}{dt} &= -\sigma \int_\Omega u_x^2 a dx \\ &\leqq -\frac{\sigma}{C_0}\int_\Omega (u-1)^2 a dx \\ &= -\frac{2\sigma}{C_0} U, \end{aligned}$$

whence

$$U(t) \leqq U(0) e^{-\epsilon t}, \; 0 < t < \infty, \tag{8.21}$$

for an $\epsilon > 0$. Finally consider (8.18), for which

$$\varphi''(\xi) = \frac{1}{\xi}$$

and

$$\frac{d\Phi}{dt} = -\sigma \int_\Omega \frac{1}{u} u_x^2 a dx. \tag{8.22}$$

Since u is bounded below, we may find a $\delta > 0$ small enough such that

$$\frac{d}{dt}(U - \delta\Phi) = -\sigma \int_\Omega u_x^2(1 - \frac{\delta}{u})adx < 0,\ 0 < t < \infty, \tag{8.23}$$

and subsequently because $U(\infty) = \Phi(\infty) = 0$, on integrating,

$$\Phi(t) \leqq \frac{1}{\delta}U(t) \leqq \frac{1}{\delta}U(0)e^{-\epsilon t},\ 0 < t < \infty. \tag{8.24}$$

The parameters occuring in (8.24) are not structural to the entropy nor even to the equation itself but depend on the particular solution at hand. This notwithstanding, the result will serve as a guide to diagnostics for the GBCD statistic.

Acknowledgements. This work is an activity of the CMU Center for Excellence in Materials Research and Innovation. This research was done while Y. Epshteyn and R. Sharp were postdoctoral associates at the Center for Nonlinear Analysis. We are grateful to our colleagues G. Rohrer, A. D. Rollett, R. Schwab, and R. Suter for their collaboration.

REFERENCES

[1] B.L. Adams, D. Kinderlehrer, I. Livshits, D. Mason, W.W. Mullins, G.S. Rohrer, A.D. Rollett, D. Saylor, S Ta'asan, and C. Wu. Extracting grain boundary energy from triple junction measurement. *Interface Science*, 7:321–338, 1999.

[2] BL Adams, D Kinderlehrer, WW Mullins, AD Rollett, and S Ta'asan. Extracting the relative grain boundary free energy and mobility functions from the geometry of microstructures. *Scripta Materiala*, 38(4):531–536, Jan 13 1998.

[3] Luigi Ambrosio, Nicola Gigli, and Giuseppe Savaré. *Gradient flows in metric spaces and in the space of probability measures*. Lectures in Mathematics ETH Zürich. Birkhäuser Verlag, Basel, second edition, 2008.

[4] Todd Arbogast. Implementation of a locally conservative numerical subgrid upscaling scheme for two-phase Darcy flow. *Comput. Geosci.*, 6(3-4):453–481, 2002. Locally conservative numerical methods for flow in porous media.

[5] Todd Arbogast and Heather L. Lehr. Homogenization of a Darcy-Stokes system modeling vuggy porous media. *Comput. Geosci.*, 10(3):291–302, 2006.

[6] Matthew Balhoff, Andro Mikelić, and Mary F. Wheeler. Polynomial filtration laws for low Reynolds number flows through porous media. *Transp. Porous Media*, 81(1):35–60, 2010.

[7] Matthew T. Balhoff, Sunil G. Thomas, and Mary F. Wheeler. Mortar coupling and upscaling of pore-scale models. *Comput. Geosci.*, 12(1):15–27, 2008.

[8] K. Barmak, E. Eggeling, M. Emelianenko, Y. Epshteyn, D. Kinderlehrer, R.Sharp, and S.Ta'asan. Predictive theory for the grain boundary character distribution. In Proc. Recrystallization and Grain Growth IV,, 2010.

[9] K. Barmak, E. Eggeling, M. Emelianenko, Y. Epshteyn, D. Kinderlehrer, R. Sharp, and S. Ta'asan. Critical events, entropy, and the grain boundary character distribution. Center for Nonlinear Analysis 10-CNA-014, Carnegie Mellon University, 2010.

[10] K. Barmak, E. Eggeling, M. Emelianenko, Y. Epshteyn, D. Kinderlehrer, and S. Ta'asan. Geometric growth and character development in large metastable systems. *Rendiconti di Matematica, Serie VII*, 29:65–81, 2009.

[11] K. Barmak, M. Emelianenko, D. Golovaty, D. Kinderlehrer, and S. Ta'asan. On a statistical theory of critical events in microstructural evolution. In *Proceedings CMDS 11*, pages 185–194. ENSMP Press, 2007.

[12] K. Barmak, M. Emelianenko, D. Golovaty, D. Kinderlehrer, and S. Ta'asan. Towards a statistical theory of texture evolution in polycrystals. *SIAM Journal Sci. Comp.*, 30(6):3150–3169, 2007.

[13] K. Barmak, M. Emelianenko, D. Golovaty, D. Kinderlehrer, and S. Ta'asan. A new perspective on texture evolution. *International Journal on Numerical Analysis and Modeling*, 5(Sp. Iss. SI):93–108, 2008.

[14] Katayun Barmak, David Kinderlehrer, Irine Livshits, and Shlomo Ta'asan. Remarks on a multiscale approach to grain growth in polycrystals. In *Variational problems in materials science*, volume 68 of *Progr. Nonlinear Differential Equations Appl.*, pages 1–11. Birkhäuser, Basel, 2006.
[15] Jean-David Benamou and Yann Brenier. A computational fluid mechanics solution to the Monge-Kantorovich mass transfer problem. *Numer. Math.*, 84(3):375–393, 2000.
[16] G. Bertotti. *Hysteresis in magnetism*. Academic Press, 1998.
[17] Eran Bouchbinder and J. S. Langer. Nonequilibrium thermodynamics of driven amorphous materials. i. internal degrees of freedom and volume deformation. *Physical Review E*, 80(3, Part 1), Sep 2009.
[18] Eran Bouchbinder and J. S. Langer. Nonequilibrium thermodynamics of driven amorphous materials. ii. effective-temperature theory. *Physical Review E*, 80(3, Part 1), Sep 2009.
[19] Eran Bouchbinder and J. S. Langer. Nonequilibrium thermodynamics of driven amorphous materials. iii. shear-transformation-zone plasticity. *Physical Review E*, 80(3, Part 1), Sep 2009.
[20] Lia Bronsard and Fernando Reitich. On three-phase boundary motion and the singular limit of a vector-valued Ginzburg-Landau equation. *Arch. Rational Mech. Anal.*, 124(4):355–379, 1993.
[21] Philippe G. Ciarlet. *The finite element method for elliptic problems*. North-Holland Publishing Co., Amsterdam, 1978. Studies in Mathematics and its Applications, Vol. 4.
[22] Albert Cohen. A stochastic approach to coarsening of cellular networks. *Multiscale Model. Simul.*, 8(2):463–480, 2009/10.
[23] Antonio DeSimone, Robert V. Kohn, Stefan Müller, Felix Otto, and Rudolf Schäfer. Two-dimensional modelling of soft ferromagnetic films. *R. Soc. Lond. Proc. Ser. A Math. Phys. Eng. Sci.*, 457(2016):2983–2991, 2001.
[24] M Frechet. Sur la distance de deux lois de probabilite. *Comptes Rendus de l' Academie des Sciences Serie I-Mathematique*, 244(6):689–692, 1957.
[25] Crispin Gardiner. *Stochastic methods, 4th edition*. Springer-Verlag, 2009.
[26] S. K. Godunov. A difference method for numerical calculation of discontinuous solutions of the equations of hydrodynamics. *Mat. Sb. (N.S.)*, 47 (89):271–306, 1959.
[27] S. K. Godunov and V. S. Ryaben'kii. *Difference schemes*, volume 19 of *Studies in Mathematics and its Applications*. North-Holland Publishing Co., Amsterdam, 1987. An introduction to the underlying theory, Translated from the Russian by E. M. Gelbard.
[28] J. Gruber, H. M. Miller, T. D. Hoffmann, G. S. Rohrer, and A. D. Rollett. Misorientation texture development during grain growth. part i: Simulation and experiment. *Acta Materialia*, 57(20):6102–6112, Dec 2009.
[29] J. Gruber, A. D. Rollett, and G. S. Rohrer. Misorientation texture development during grain growth. part ii: Theory. *Acta Materialia*, 58(1):14–19, Jan 2010.
[30] M. Gurtin. *Thermomechanics of evolving phase boundaries in the plane*. Oxford, 1993.
[31] R. Helmig. *Multiphase flow and transport processes in the subsurface*. Springer, 1997.
[32] C. Herring. Surface tension as a motivation for sintering. In Walter E. Kingston, editor, *The Physics of Powder Metallurgy*, pages 143–179. Mcgraw-Hill, New York, 1951.
[33] C. Herring. The use of classical macroscopic concepts in surface energy problems. In Robert Gomer and Cyril Stanley Smith, editors, *Structure and Properties of Solid Surfaces*, pages 5–81, Chicago, 1952. The University of Chicago Press. Proceedings of a conference arranged by the National Research Council and held in September, 1952, in Lake Geneva, Wisconsin, USA.
[34] EA Holm, GN Hassold, and MA Miodownik. On misorientation distribution evolution during anisotropic grain growth. *Acta Materialia*, 49(15):2981–2991, Sep 3 2001.
[35] Arieh Iserles. *A first course in the numerical analysis of differential equations*. Cambridge Texts in Applied Mathematics. Cambridge University Press, Cambridge, 1996.
[36] R Jordan, D Kinderlehrer, and F Otto. Free energy and the fokker-planck equation. *Physica D*, 107(2-4):265–271, Sep 1 1997.
[37] R Jordan, D Kinderlehrer, and F Otto. The variational formulation of the fokker-planck equation. *SIAM J. Math. Analysis*, 29(1):1–17, Jan 1998.
[38] D Kinderlehrer, J Lee, I Livshits, A Rollett, and S Ta'asan. Mesoscale simulation of grain growth. *Recrystalliztion and grain growth, pts 1 and 2*, 467-470(Part 1-2):1057–1062, 2004.
[39] D Kinderlehrer and C Liu. Evolution of grain boundaries. *Mathematical Models and Methods in Applied Sciences*, 11(4):713–729, Jun 2001.

[40] D Kinderlehrer, I Livshits, GS Rohrer, S Ta'asan, and P Yu. Mesoscale simulation of the evolution of the grain boundary character distribution. *Recrystallization and grain growth, pts 1 and 2*, 467-470(Part 1-2):1063–1068, 2004.

[41] David Kinderlehrer, Irene Livshits, and Shlomo Ta'asan. A variational approach to modeling and simulation of grain growth. *SIAM J. Sci. Comp.*, 28(5):1694–1715, 2006.

[42] Robert V. Kohn and Felix Otto. Upper bounds on coarsening rates. *Comm. Math. Phys.*, 229(3):375–395, 2002.

[43] L. D. Landau and E. M. Lifshitz. *Fluid mechanics*. Translated from the Russian by J. B. Sykes and W. H. Reid. Course of Theoretical Physics, Vol. 6. Pergamon Press, London, 1959.

[44] Peter D. Lax. Weak solutions of nonlinear hyperbolic equations and their numerical computation. *Comm. Pure Appl. Math.*, 7:159–193, 1954.

[45] Peter D. Lax. *Hyperbolic systems of conservation laws and the mathematical theory of shock waves*. Society for Industrial and Applied Mathematics, Philadelphia, Pa., 1973. Conference Board of the Mathematical Sciences Regional Conference Series in Applied Mathematics, No. 11.

[46] Bo Li, John Lowengrub, Andreas Rätz, and Axel Voigt. Geometric evolution laws for thin crystalline films: modeling and numerics. *Commun. Comput. Phys.*, 6(3):433–482, 2009.

[47] I.M. Lifshitz, E. M. and V.V. Slyozov. The kinetics of precipitation from suprsaturated solid solutions. *Journal of Physics and Chemistry of Solids*, 19(1-2):35–50, 1961.

[48] John S. Lowengrub, Andreas Rätz, and Axel Voigt. Phase-field modeling of the dynamics of multicomponent vesicles: spinodal decomposition, coarsening, budding, and fission. *Phys. Rev. E (3)*, 79(3):0311926, 13, 2009.

[49] MA Miodownik, P Smereka, DJ Srolovitz, and EA Holm. Scaling of dislocation cell structures: diffusion in orientation space. *PROCEEDINGS OF THE ROYAL SOCIETY A-MATHEMATICAL PHYSICAL AND ENGINEERING SCIENCES*, 457(2012):1807–1819, Aug 8 2001.

[50] W.W. Mullins. *Solid Surface Morphologies Governed by Capillarity*, pages 17–66. American Society for Metals, Metals Park, Ohio, 1963.

[51] W.W. Mullins. On idealized 2-dimensional grain growth. *Scripta Metallurgica*, 22(9):1441–1444, SEP 1988.

[52] Felix Otto, Tobias Rump, and Dejan Slepčev. Coarsening rates for a droplet model: rigorous upper bounds. *SIAM J. Math. Anal.*, 38(2):503–529 (electronic), 2006.

[53] GS Rohrer. Influence of interface anisotropy on grain growth and coarsening. *Annual Review of Materials Research*, 35:99–126, 2005.

[54] Anthony D. Rollett, S.-B. Lee, R. Campman, and G. S. Rohrer. Three-dimensional characterization of microstructure by electron back-scatter diffraction. *Annual Review of Materials Research*, 37:627–658, 2007.

[55] DM Saylor, A Morawiec, and GS Rohrer. The relative free energies of grain boundaries in magnesia as a function of five macroscopic parameters. *Acta Materialia*, 51(13):3675–3686, AUG 1 2003.

[56] Cyril Stanley Smith. Grain shapes and other metallurgical applications of topology. In *Metal Interfaces*, pages 65–108, Cleveland, Ohio, 1952. American Society for Metals, American Society for Metals.

[57] H. Bruce Stewart and Burton Wendroff. Two-phase flow: models and methods. *J. Comput. Phys.*, 56(3):363–409, 1984.

[58] Andrea Toselli and Olof Widlund. *Domain decomposition methods—algorithms and theory*, volume 34 of *Springer Series in Computational Mathematics*. Springer-Verlag, Berlin, 2005.

[59] Cédric Villani. *Topics in optimal transportation*, volume 58 of *Graduate Studies in Mathematics*. American Mathematical Society, Providence, RI, 2003.

[60] J. Von Neumann and R. D. Richtmyer. A method for the numerical calculation of hydrodynamic shocks. *J. Appl. Phys.*, 21:232–237, 1950.

[61] C Wagner. Theorie der alterung von niederschlagen durch umlosen (Ostwald-Reifung). *Zeitschrift fur Elektrochemie*, 65(7-8):581–591, 1961.

Received xxxx 20xx; revised xxxx 20xx.

E-mail address: katayun@andrew.cmu.edu
E-mail address: eva.eggeling@fraunhofer.at
E-mail address: memelian@gmu.edu
E-mail address: epshteyn@math.utah.edu
E-mail address: davidk@cmu.edu
E-mail address: sharp@andrew.cmu.edu
E-mail address: shlomo@andrew.cmu.edu